Available online at www.sciencedirect.com
SCIENCE DIRECT®
Journal of Magnetic Resonance 177 (2005) 261–273
JMR Journal of Magnetic Resonance
www.elsevier.com/locate/jmr

Dielectric resonator-based resonant structure for sensitive ESR measurements at high-hydrostatic pressures

Andrzej Sienkiewicz [a,b,*], Bertrand Vileno [a], Slaven Garaj [a], Marek Jaworski [b], László Forró [a]

[a] Institute of Physics of Complex Matter, Ecole Polytechnique Fédérale de Lausanne, Lausanne, CH-1015, Switzerland
[b] Institute of Physics, Polish Academy of Sciences, Al. Lotników 32/46, 02-668 Warsaw, Poland

Received 20 June 2005; revised 9 August 2005
Available online 15 September 2005

Abstract

We present a newly developed microwave probe head that accommodates a gasketed sapphire anvil cell (SAC) for performing sensitive electron spin resonance (ESR) measurements under high-hydrostatic pressures. The system was designed around commercially available dielectric resonators (DRs) having the dielectric permittivity of ~30. The microwave resonant structure operates in a *wide-stretched* double-stacked geometry and resonates in the lowest cylindrical *quasi* TE_{011} mode around 9.2 GHz. The most vital parts of the probe's microwave heart were made of plastic materials, thus making the resonant structure transparent to magnetic field modulation at 100 kHz. The overall ESR sensitivity of the probe was demonstrated for a small speck of 2,2-diphenyl-1-picrylhydrazyl radical (DPPH) positioned in the gasket of the SAC, using water as the pressure-transmitting medium. The system was also used for studying pressure-induced changes in spin-relaxation mechanisms of a *quasi*-1D-conducting polymer, K_1C_{60}. For small samples located in the sample hole of the gasket the probe reveals sensitivity that is only ~3 times less than that yielded by regular ESR cavities.

Keywords: Cw-X-band ESR; Dielectric resonator; High-hydrostatic pressure; Sapphire anvil cell

1. Introduction

The potential of combining ESR with high-hydrostatic pressures has been early and widely recognized [1–3]. The high-pressure ESR studies can provide a wealth of information about the spin system, since all the principal quantities associated with the spin dynamics, such as line shape and its intensity, spectroscopic *g*-, *D*-, and *A*-factors, the ESR linewidth, ΔH_{pp}, and the spin-relaxation times T_1 and T_2 are sensitive to variable pressure. Usually, the most dramatic changes in the spin dynamics occur at crystallographic and magnetic phase transitions that are sensitive to the pressure-induced changes in the interatomic distances.

Typical phenomena of this type are the transitions from the paramagnetic to the antiferromagnetic state, transition from insulating to conducting state, or formation of a polymeric type of interatomic binding. The major technical problem in designing high-hydrostatic pressure ESR systems is related to coupling microwaves to sealed and pressure-resistant metallic vessels. In ordinary commercial ESR systems, the interaction of electronic spins with the oscillatory electromagnetic field occurs in resonant cavities operating in the microwave frequency range. The major rationale for using cavities is to increase the intensity of the magnetic component, H_1, of the incident electromagnetic radiation at the sample space.

The early high-pressure ESR systems employed modified cylindrical [4–7] or coaxial [8] cavities that were entirely filled with low-loss, high-purity dielectric material, such as quartz (fused SiO_2), mono-crystalline sapphire or alumina ceramics (Al_2O_3). Implementation of the dielectric filling enabled one to reduce the overall size of microwave cavities operating at

* Corresponding author. Fax: +48 22 843 09 26.
E-mail addresses: sienk@ifpan.edu.pl, sienkiew@igahpse.epfl.ch (A. Sienkiewicz).

1090-7807/$ - see front matter © 2005 Elsevier Inc. All rights reserved.
doi:10.1016/j.jmr.2005.08.002

high pressure, since the overall cavity dimensions could be scaled down as $1/\sqrt{\varepsilon_r}$, where ε_r denotes the relative dielectric permittivity of the filling material. Generally, microwave cavities employed in such systems operated in cylindrical TE_{011}, TE_{111} or TE_{112} modes. The presence of dielectric, prerequisite to reduce the cavity overall size, made also incorporation of the microwave resonant structures into pressure-resistant chambers considerably easier. The dielectric filling played also a beneficial role in reducing the overall volume of the pressure-transmitting medium.

Beryllium bronze (BeCu), being strictly non-magnetic and having excellent mechanical properties, was often employed for manufacturing the pressure-resistant external shell. At higher pressures (above 1 GPa), the external dimensions of the pressure-resistant metallic chamber as well as engineering difficulties and danger were the most critical limitations of such conventional ESR probe heads. Furthermore, thick walls of the bulky pressure vessels, being non-transparent to the standard magnetic field modulation, precluded application of the commonly used high-frequency magnetic field modulation, even in the recent versions of such systems [9]. To circumvent this problem, more complex microwave cavities operating in higher cylindrical modes have been proposed [10–12]. The entire volume of such elongated cylindrical cavities was filled with two different dielectric materials of high purity (fused quartz and sapphire). The quartz filling accommodated the sample compartment and a small modulation coil, whereas sapphire filling served both as a part of the resonant structure and as a pressure-resistant plug. Such systems have revealed practical sensitivity and have been successfully used in many ESR experiments at pressures up to ~0.7 GPa [13–17].

The upper pressure limit of ca. 6–8 GPa for the cavity-based ESR high-pressure systems was established while using a solid pressure-transmitting medium and a set of Bridgman-type anvils made of Al_2O_3 that were directly incorporated into the resonant cavity [18–20].

Over the last two decades, the general high-pressure experimentation has been revolutionized by various versions of a diamond-anvil cell (DAC) [21–24]. The DAC consists of two diamond culets that are separated by a metallic gasket and operates in the so-called opposed-anvil (or Bridgman) configuration. The DAC is also much safer than standard equipment. Since diamond is transparent to photons over a wide range of electromagnetic radiation, the DAC-based pressure systems are particularly suitable for performing optical investigations, from direct light-scattering techniques such as Raman scattering [25,26], to Brillouin scattering [27], and X-ray diffraction [28,29]. With only minor modifications, this technique has also been used for various dc- and ac-impedance studies [30,31]. Experiments in the DACs have been carried out over an ultra-wide range of hydrostatic pressures reaching ~500 GPa [32,33]. Sapphire-anvil cell (SAC), a parent and considerably cheaper modality of DAC, has been used at lower pressures (up to ~10 GPa) [34].

In spite of its potential, implementation of the diamond-anvil or sapphire anvil cells in ESR technique has not become greatly popularized. Commercially available ESR spectrometers that operate in X-band and at atmospheric pressure are usually equipped with metallic-wall cavities whose dimensions are comparable to the microwave free-space wavelength, λ_f, of ~3 cm. Since typical DAC or SAC are roughly of the same size as λ_f, the topological constraints imposed by cavity modal distribution patterns prohibit the simple insertion of the high-pressure anvil cell into the sample space of a typical resonant cavity. To date, there have only been two attempts of combining the gasketed diamond-anvil cells with the ESR probe heads.

First, in 1985, Sakai and Pifer incorporated a regular DAC into a section of a tunable-shorted X-band waveguide and performed ESR measurements at high-hydrostatic pressures up to 10 GPa [35]. In this pioneering design, a BeCu-made gasket, an inherent part of the DAC, functioned also as a linear microwave resonator. The gasket was rectangular in shape with its approximate length of ~12 mm, which roughly corresponded to $\lambda_f/2$. Thus, the gasket-resonator could directly be coupled to the microwave field propagating through the waveguide. The drawback of this design was related to an inherently low resonator quality factor ($Q_L \sim 300$) of the linear resonator, thus leading to a rather low sensitivity of the system.

In 1992, a combination of the DAC with a miniature microwave resonant structure designed around high-dielectric ceramics was explored by Bromberg and Chan [36]. Such ceramic elements, which are often referred to as dielectric resonators (DRs), confine the electromagnetic fields to their own geometry rather than to the external metallic case. This results in a substantial size reduction as well as in lower radiation and conduction loss. Recently, ceramic materials having high-relative permittivity ($\varepsilon_r > 20$) and low dielectric loss tangent (e.g., $1/\tan\delta > 10{,}000$ at 10 GHz) are extensively used in the design of microwave resonators, oscillators, and filters [37,38]. In ESR applications, the DR-based systems offer much larger filling factors, η, than commonly used metallic-wall cavities [39–43]. Bromberg and Chan took advantage of this fact while combining a standard Merrill–Bassett diamond-anvil cell with a double-stacked dielectric resonator. Their microwave resonant structure was built around two custom-made high-dielectric pellets of TiO_2 having $\varepsilon_r \sim 100$. A rather large spacing of 4.5 mm between two coupled DRs made it possible to accommodate the essential parts of a DAC (including the metallic gasket) in the ESR-active volume of the resonant structure. The microwave resonant structure operated in its lowest axially symmetric cylindrical TE mode. This most commonly used resonant mode in dielectric resonators is topologically equivalent to the lowest TE_{011} mode of a cylindrical cavity and is classified as $TE_{01\delta}$ mode (where δ is a real number assuming values in the range 0.5–1.0) or as *quasi* TE_{011} mode, reflecting the fact that the topology of the mode extends beyond the high-dielectric material. (The name *quasi* TE_{011} will be used

throughout this paper regarding the lowest axially symmetric mode of the DR.) In their report, Bromberg and Chan demonstrated that the tangential magnetic component, H_1, was reasonably strong at the gasket hole, thus enabling one to perform high-pressure ESR measurements.

In this work, we report a novel high-pressure ESR probe that combines a double-stacked DR resonant structure with a sapphire anvil cell (SAC). In contrast to the design of Bromberg and Chan, the microwave resonant structure of our system was developed around commercially available ceramic DRs having the relative dielectric permittivity considerably lower ($\varepsilon_r \sim 30$). The design reported here also employs an entirely different pattern of the microwave coupling, which is based on a fixed magnetic dipole (antenna) that is assembled with a variable tuner. This also distinguishes our design from the solution adopted by Bromberg and Chan whose system was not remotely tunable.

Furthermore, the resonant structure in the present design was build from plastic materials. Therefore it is transparent to the magnetic field modulation frequency at 100 kHz, which substantially improves the overall sensitivity of the system. The DR-based system equipped with sapphire anvils practically triples the upper pressure limit as reference to our helium-gas operating high-pressure ESR probes [10,15], reaching pressures up to ~2 GPa.

The newly developed probe has already been employed to study pressure-induced phase transition from ferromagnetic to paramagnetic state in an organic charge-transfer compound, TDAE-C_{60} [44]. Here, we describe technical details and show performance of the DR-based high-pressure ESR probe while following pressure-induced spin-relaxation changes in a *quasi*-1D-conducting polymer, K_1C_{60}. Since we were able to acquire ESR spectra while using water as the pressure-transmitting medium, we emphasize a potential of the newly designed probe for performing high-pressure ESR studies of aqueous samples or samples suspended in aqueous milieus.

2. Technical description of the dielectric-resonator-based high-pressure ESR probe

2.1. General overview

We designed a high-pressure ESR probe that cooperates with a commercial X-band ESR spectrometer, Model ESP 300 E (Bruker Analytik GmbH, Germany). It connects to the spectrometer's microwave bridge simply by replacing a standard ESR cavity.

The high-pressure DR-based ESR probe consists of three major components:

1. DR-based microwave resonant structure;
2. High-pressure-generating cell containing the sapphire anvils cell (SAC);
3. Beryllium bronze (BeCu)-made body that accommodates the microwave resonant structure and provides guidance for the two pistons of the SAC.

Similar to the design of Bromberg and Chan [36], our ESR probe was constructed around a double-stacked DR configuration resonating in the *quasi* TE_{011} mode with the axial magnetic H_1 component oriented horizontally and perpendicular to the external magnetic field, H_0. The double-stacked *wide-stretched* configuration of the DRs provides an easy access through the spacing between the resonators, thus enabling one to insert a complete DAC or SAC directly into the active zone of the resonant structure. Such configuration makes it possible to assemble the microwave resonant structure with a pressure-generating cell having anvils operating along the vertical axis of the device.

The vertical cross-sectional views of the high-pressure ESR probe in the planes perpendicular and parallel to the external magnetic field (H_0) are shown Fig. 1.

2.2. DR-based microwave resonant structure

Generally, we oriented the DR-based microwave part of our design according to the technology described in detail in [41–43] and recently adopted also by Lassmann et al. [45].

The microwave heart of the probe head was built around two commercially available DRs from MuRata Ageltro Electronics AG, Mönchaltorf, Switzerland. These high-dielectric elements from the MuRata Resomics^R Dielectric Resonators 'R' Series (Model DRT065R020C029A) have dielectric constant $\varepsilon_r \sim 29.7$ and a low-dielectric loss tangent, $\tan\delta = 6.6 \times 10^{-5}$ at 10 GHz. The DRs are cylindrical in shape and have the following dimensions: 6.50-mm OD, 2.0-mm ID, and 2.88-mm height. A single DR having such dimensions resonates in its fundamental *quasi* TE_{011} mode at 9.08 GHz, whereas a double-stacked configuration with separation of 4.5 mm resonates at 9.19 GHz [42].

Two dielectric resonators are located inside a cylindrical element manufactured from Rexolite (Rexolite^R 1422 from C-Lec Plastics, NJ, USA). Rexolite is a cross-linked polystyrene polymer with a small dielectric constant ($\varepsilon_r = 2.53$) and low-dielectric loss ($\tan\delta = 6.6 \times 10^{-4}$). The Rexolite-made cylinder, herein referred to as 'resonator body,' having dimensions 12.7-mm OD, 6.55-mm ID, and 15.4-mm length, is schematically shown in Fig. 2. The outer surface of the resonator body was silver-coated with a thin layer of silver paint (DuPont de Nemours, USA, product number # 4817N), which provided an adequate microwave shielding for the resonant structure.

The thickness of silver coating was approximately in the range from 25 to 50 μm, thus being larger than the skin depth of the microwave field, $d_{\mu w} = 0.67$ μm (at 9.6 GHz for metallic silver) and considerably less than the skin depth of the modulation field, $d_m = 203$ μm (at 100 kHz). Two 4.6-mm diameter holes drilled along the axis perpendicular to the cylindrical axis of the resonator body served as openings to accommodate sapphire anvils (**1a** and **1b** in Fig. 2). The 3.6-mm diameter hole (**3** in Fig. 2), drilled also

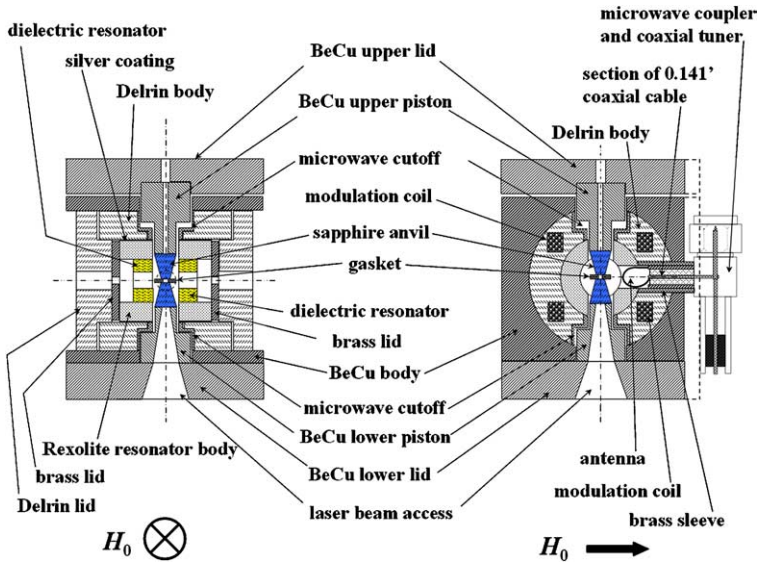

Fig. 1. Simplified cross-sectional view of the high-pressure ESR probe including the microwave coupler and coaxial tuner. The cross-sectional schemes are shown in the planes perpendicular and parallel to the external magnetic field H_0, on the left-hand side and right-hand side of the drawing, respectively.

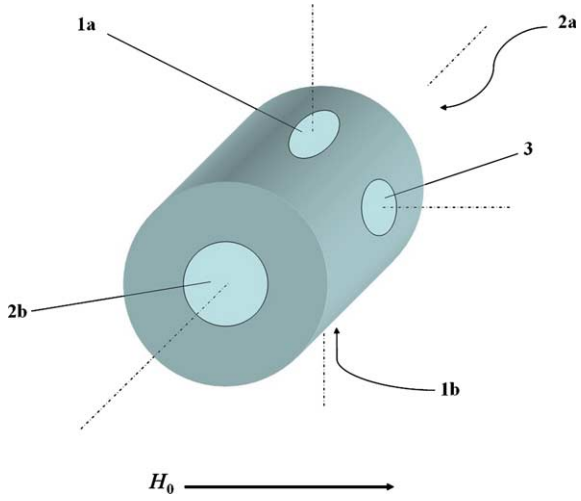

Fig. 2. Schematic view of the Rexolite-made resonator body: **1a** and **1b** are cylindrical 4.6-mm diameter holes providing upper and lower entrances for inserting sapphire anvils; **2a** and **2b** are openings of the cylindrical 6.55-mm diameter hole (drilled through along the cylindrical axis), which provide two entrances for inserting the DRs; **3** is the cylindrical 3.6-mm diameter hole to accommodate the coupling antenna.

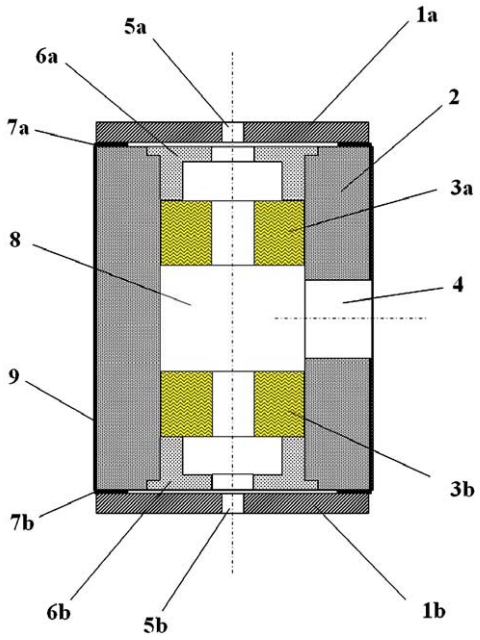

Fig. 3. Cross-sectional view of the resonant structure. **1a** and **1b** gold-plated brass disks (microwave shielding); **2** Rexolite-made resonator body; **3a** and **3b** dielectric resonators; **4** cylindrical entrance for the antenna; **5a** and **5b** entrances for capillaries containing test samples; **6a** and **6b** Rexolite-made spacers; **7a** and **7b** silver gaskets (microwave shielding); **8** part of the ESR-active volume accommodating sapphire anvils and the gasket; **9** silver-paint coating (microwave shielding).

along the perpendicular axis to the cylindrical axis of the resonator body and oriented at 90° angle with reference to the axis of the holes **1a** and **1b**, served as the entrance port for the coupling antenna.

The cross-sectional view of the resonant structure consisting of the Rexolite-made resonator body, dielectric resonators and microwave shielding is schematically shown in Fig. 3. As can be seen in this figure, the final location of the DRs inside the resonator body is defined by two cylindrical spacers (6.5-mm OD, 2.0-mm ID, and 2.4-mm thick) also made from Rexolite (**6a** and **6b** in Fig. 3). Before inserting into the resonator body, the DRs were pre-assembled with the Rexolite spacers using a tiny amount of acrylic glue. Two gold-plated disks (**1a** and **1b** in Fig. 3), made from non-magnetic brass (1-mm thick) served as a final closure of the resonant structure on both sides of the cylindrical resonator body. Two thin washers (**7a** and **7b** in Fig. 3) made from 25-μm silver foil ensured good electrical contact between the silver coating and brass disks.

The ESR-active volume in the spacing between the DRs (**8** in Fig. 3) accommodates the sapphire anvils and the gasket. Two 1-mm diameter cylindrical holes (**5a** and **5b** in Fig. 3) drilled in the brass disks serve as auxiliary entrances for inserting capillaries containing test samples.

The outer protective shell of the resonant structure is made from a robust polyester material, Delrin^{R} (GoodFellow, Knoxville, TN, USA). Delrin may easily be machined to precise dimensions and has superior mechanical properties, including high strength and rigidity over a broad temperature range, toughness, and resistance to repeated temperature cycling. The outer protective shell made from Delrin is referred to as the Delrin body (Fig. 1). The resonant structure precisely fits into the cylindrical hole of the Delrin body. The pattern of the openings drilled in the lateral wall of the Delrin body exactly corresponds to the pattern of respective cylindrical holes of the resonator body. Two 10.5-mm diameter cylindrical openings in the Delrin body serve as guiding elements for the BeCu pistons (see Fig. 1). These openings are equipped with metallic cladding, which provides cutoff for microwave radiation. The microwave cutoff elements, manufactured as short sections of brass-made tubes (with a stepwise change of the inner diameter), were pressed into the Delrin body (Fig. 1). The remaining 5.5-mm cylindrical hole drilled in the lateral wall of the Delrin body serves as the guiding entrance for the antenna.

Two sets of four equally spaced brass M2.5 screws serve to firmly attach the Delrin-made lids to both sides of the Delrin body. The Delrin lids (shown in the left-hand side portion of Fig. 1) push the brass microwave shielding discs against the resonator body. They also crush silver-foil gaskets (25-μm thick) on both sides of the resonator body (**7a** and **7b** in Fig. 3). This ensures good mechanical and electrical contacts between the silver coating of the resonator body and the gold-plated brass disks.

The rectangular grooves milled in the cylindrical wall of the Delrin body accommodate modulation coils (right-hand portion of Fig. 1). The impedance of these coils ($R = 3.1\ \Omega$ and $L = 240\ \mu H$), fairy close to the impedance of a standard TE_{102} cavity, enables one to connect them directly to the 100 kHz amplifier of the Bruker ESP300E spectrometer. Before performing measurements, the coils were calibrated using a standard ESR line-broadening procedure. A small speck of DPPH, inserted into the sample volume in the cylindrical hole of the gasket, was used as a reference sample.

The final spacing between the DR was set to 4.8 mm. The empty resonant structure of this topology resonated around 9.30 GHz. This resonant frequency is by ~0.1 GHz higher than that reported previously for a similar double-stacked DR [42]. The observed enhancement of the resonant frequency is due to a close location of the DRs to the shielding brass disks (2.4 mm in the present design). Upon insertion of the gasket and sapphire anvils, the resonant frequency diminishes to ~9.20 GHz. The measured loaded quality factor Q_L of the empty resonant structure was ~2500. Upon loading the pistons, the sapphire anvils, and the gasket, the Q_L-factor dropped to ~1200–1300. The measurements of the Q_L-factor were performed in the reflection mode using a bench test microwave bridge designed around the HP8350B sweep oscillator equipped with HP83545A plug-in (5.9–12.4 GHz microwave source) and containing the HP537A cavity wavemeter. Q-factors were determined from $f_0/\Delta f$, where f_0 is the resonator resonant frequency and Δf is 3-dB bandwidth. The observed changes in the resonant frequency and resonator Q_L-factor can be associated to the presence of the dielectric load (sapphire anvils) and of the remaining metallic parts of the SAC, i.e., the gasket and terminations of the pistons, in the active volume of the resonant structure.

The outermost part of the ESR probe was manufactured from beryllium bronze (BeCu) rod having 50 mm in diameter and 38 mm in length. As mentioned before, BeCu is a non-magnetic, copper alloy. However, unlike pure copper, beryllium–bronze can be heat treated to harden the alloy into an extremely strong and durable metal. Elements made from BeCu are commonly used at cryogenic temperatures where, unlike other copper alloys, they do not become brittle. BeCu is also a material of choice for designing mechanical parts that accommodate regular diamond or sapphire anvil high-pressure cells.

The element made of BeCu is referred to as the BeCu body (Fig. 1). The cylindrical opening (22.5 mm in diameter) drilled perpendicular to the longitudinal axis of the BeCu body accommodates the resonant structure protected by the Delrin body. The 10.05-mm diameter hole drilled along the BeCu longitudinal axis provides mechanical guidance for the BeCu pistons of the pressure-generating cell. The lateral groove milled in the BeCu body provides guidance and attachment site for the microwave coupler and coaxial tuner (shown in right-hand side of Fig. 1). This latter element, which is also integrated with the antenna, enables one to critically couple the resonant structure. A linear actuator (not shown in Fig. 1) can be used for remote tuning of the system.

The coupling mechanism was built around a modified SMA right-angle connector, Model 16 SMA-50-3-3/111 QE, from Huber & Suhner SA (Herisau, Switzerland). This element integrates the antenna with the coaxial tuner and provides an entry port for microwaves via the SMA male-type connector. The coupling loop of the antenna was formed from a short section of a silver-cladded copper wire (0.61 mm in diameter, from Huber & Suhner AG, Herisau, Switzerland). Before forming the antenna, the copper wire was slightly rigidified by pulling. The dimensions of the elongated loop of the antenna were: 6.5-mm total length and 1.25-mm inner radius. Both terminations of the antenna loop were soldered to the attachment sites made on one end of 7.0-mm long section of the copper-jacketed 0.141″ semi-rigid coaxial cable (EZ141-Cu from EZ Form Cable, Hamden, CT). The location of this element within the microwave coupler is shown in the right panel of Fig. 1. Before making the antenna anchoring sites,

the strip lengths for the center conductor of this short section of semi-rigid cable were set to 3.0 mm. The antenna anchoring sites were prepared by milling off one half of the thickness of the center conductor at the length of ~1.7 mm and by making 0.65-mm wide, 0.5-mm deep, and ~4.0-mm long groove in the copper jacket. These anchoring sites for the antenna loop can be seen in Fig. 4, where the short section of the semi-rigid 0.141″ coaxial cable is shown adjacent to the fully assembled microwave coupler. A similar anchoring site was also made on the opposite of end of the center conductor of this short semi-rigid 0.141″ coaxial cable. As shown in Fig. 4, this latter anchoring site has its plane twisted 90° as reference to the step milled to accommodate the antenna. This stepwise change in diameter of the center conductor of 0.141″ cable served as an anchoring site to accommodate the upper termination of the center conductor of the coaxial tuner (Fig. 1).

As can be seen in Fig. 4, only ~4.5-mm long portion of the antenna loop extends beyond the brass-made sleeve. This latter element protects the antenna during the process of assembly and disassembly of the high-pressure probe. The antenna's plane is coplanar with the flat surface of the DRs and excites the symmetrical *quasi* TE_{011} mode. The hexagonal threaded nut (the upper part of the SMA connector) enables one to attach the microwave coupler to a straight section of either 0.141″ copper-jacketed semi-rigid coaxial (EZ141-Cu) or 0.145″ stainless-steel semi-rigid coaxial cable. These semi-rigid cable sections are interchangeable and measure 350 mm in length, which corresponds roughly to the distance between the cryostat flange and the resonator. Under cryogenic conditions, stainless-steel cable has better thermal insulation and mechanical properties than its copper-jacketed semi-rigid equivalent, and was preferentially chosen while assembling the system for performing high-pressure ESR studies at low temperatures. The section of stainless-steel cable was purchased assembled with appropriate non-magnetic SMA connectors from SSI Cable, Shelton, WA. Above the cryostat flange, the microwaves were routed to the microwave bridge using a section of copper-jacketed EZ141-Cu cable (~600-mm long). The lower portion of 0.145″ coaxial stainless-steel cable assembled with the microwave coupler can be seen in Fig. 4.

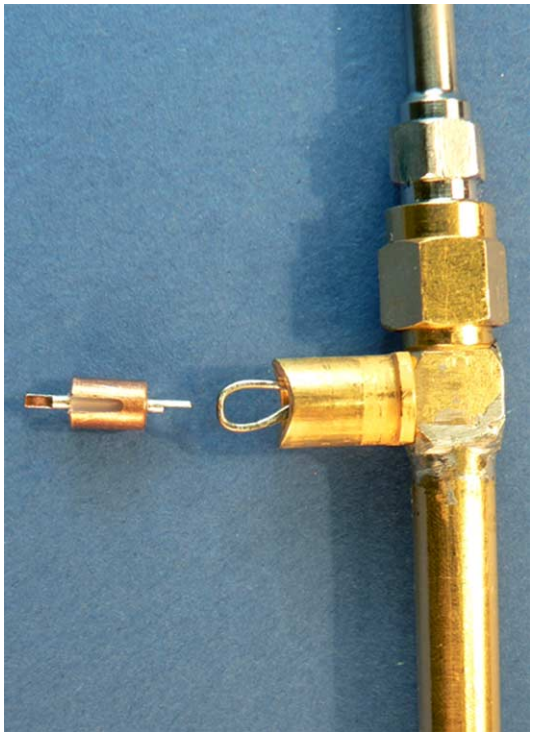

Fig. 4. The central part of the assembled microwave coupler. The short section of the copper-jacketed 0.141″ semi-rigid coaxial cable that connects the antenna loop to the center conductor of the SMA right-angle connector is shown adjacent to the antenna loop. The anchoring sites for the antenna are visible on the left end of the semi-rigid cable.

The assembly consisting of the antenna, coaxial tuner, and section of 0.145″ stainless-steel coaxial cable can be easily attached and detached to and from the BeCu body. This feature facilitates the assembly of the probe head, especially when the sample loading procedure requires anaerobic conditions (for instance, when sample loading is performed in a glove-box).

Worthy of notice is that the assembly of the resonant structure and Delrin body can be used, by itself, as a fully self-standing ESR probe head that can operate with the magnetic component H_1 oriented either vertically or horizontally, being still, however, perpendicular to the external field H_0. We found this feature was very useful while developing and testing the resonant structure before combining it with the rest of the high-pressure ESR probe.

2.3. High-pressure-generating cell containing sapphire anvils (SAC)

The sapphire anvil cell consists of two vertically oriented metallic pistons (made of gold-plated BeCu), two sapphire anvils, and the metallic gasket. The essential elements of the SAC are schematically shown in Fig. 1. The sapphire anvils were purchased from Stecher SA (Gwatt, Switzerland). The anvils were manufactured from pure Al_2O_3 crystals in the form of truncated cones, with the crystalline ***c***-axis parallel to the cone's axis. The anvils had the following dimensions: 3.95-mm table diameter, 1.9-mm culet diameter, and 4-mm height. Commercial cyanoacrylic glue for non-porous materials, Pattex^R from Henkel & Cie AG (Pratteln, Switzerland), was used to assemble the anvils with the BeCu pistons.

The metallic gasket for the SAC was manufactured from non-magnetic brass in a form of a flat cylindrical washer. The gasket's dimensions were: 3.9-mm OD, 0.5–0.9-mm ID, and 0.45–0.6-mm thickness. The cylindrical hole in the gasket together with sapphires' culets forms the sample compression chamber. The available sample volume in the compression chamber depends on the gasket's thickness and ID. For the majority of results presented in this work

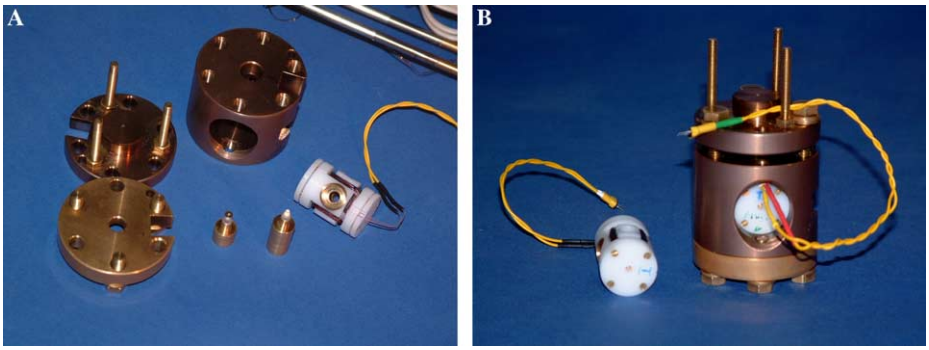

Fig. 5. (A) The partially disassembled high-pressure DR-based ESR probe. The microwave resonant structure is located in the Delrin body (white Delrin-made cylinder). The large opening visible in the upper part of the Delrin body serves as the entrance port for the piston-anvil assembly and as the microwave cutoff element. Two BeCu pistons assembled with sapphire anvils are shown adjacent to the Delrin body. The lower sapphire anvil is shown assembled with the pressure gasket. The bulky metallic elements are: BeCu body and two BeCu lids. (B) Assembled high-pressure DR-based ESR probe. An additional microwave resonant structure (inside the Delrin body) is shown adjacent to the fully assembled probe.

the sample volume was of ~0.3 μL. Before loading the sample, we found it useful to pre-assemble the gasket with the lower sapphire anvil using a small amount of acrylic glue. Different pressure-transmitting media were used, including water, paraffin oil, and mixtures of methanol and ethanol.

The high-pressure cell operates by pushing the opposite BeCu pistons assembled with sapphire anvils upon each other, which results in compressing the gasket and reducing the sample volume. In the design presented here, the lower BeCu anvil is fixed, whereas forcing the upper BeCu piston generates pressure. This is achieved with the BeCu upper lid (Fig 1), which precisely accommodates the non-supported part of the upper BeCu piston. A set of six M6 screws (also made from beryllium bronze) is used to force the BeCu upper lid, thus resulting in generation of pressure. The upper pressure limit of ~2 GPa for the present design was mainly imposed by the shape and quality of sapphire anvils (we used cheap, ca. $10.0 a pair, non-beveled anvils with sharp edges). The photographs of the partially disassembled and assembled high-pressure ESR probe are shown in Figs. 5A and B, respectively. The microwave resonant structure shown in Fig. 5A is inserted into the Delrin body. One of the microwave cutoff elements as well as the 100 kHz modulation coils, incorporated into the Delrin body, can also be recognized in Fig. 5A. The sapphire anvils shown in Fig. 5A are assembled with the BeCu pistons. The lower sapphire anvil is shown to be assembled with the gasket. The blow-up of the pistons of the SAC assembled with sapphire anvils is shown in Fig. 6.

The fully assembled probe is shown in Fig. 5B. Adjacent to the fully assembled probe a spare resonant structure is also shown. We found it useful to have several resonant structures ready for exchange while performing the high-pressure ESR experiments. In particular, in the case of paramagnetic contamination due to a leaking gasket, a spare one could quickly replace the contaminated microwave resonant structure. This operation, however, could only be performed after releasing pressure and removing the BeCu pistons and sapphire anvils from the BeCu body. When assembled with the pistons and the upper and lower

Fig. 6. The pistons of the SAC assembled with sapphire anvils. The lower sapphire anvil is assembled with the gasket. Inset: blow-up of the 0.5 mm sample hole in the gasket. The small speck of DPPH (wrapped up in a flake of PTFE tape) is shown adjacent to the crystal of ruby.

BeCu lids, the overall height of the BeCu body of the high-pressure ESR probe is of 60 mm (Fig. 5B). There is a large conical hole in the center of the lower BeCu lid, which serves as a laser-beam access for pressure calibration. The laser light penetrates through this opening to the conical hole of the BeCu lower piston and illuminates a small crystal of ruby positioned in the sample hole of the gasket (see inset to Fig. 6). This enables one to calibrate pressure in the sample volume of the gasket, as discussed in Section 3.

The high-pressure ESR probe integrated with its suspension and with the microwave coaxial cable attached to the resonant structure is shown in Fig. 7. As can be seen, the assembled BeCu body, which contains the DR-based resonant structure and the SAC, is attached to the flange of a commercial continuous gas-flow cryostat, Model CF1200 from Oxford Instruments, Oxon, England. Three threaded

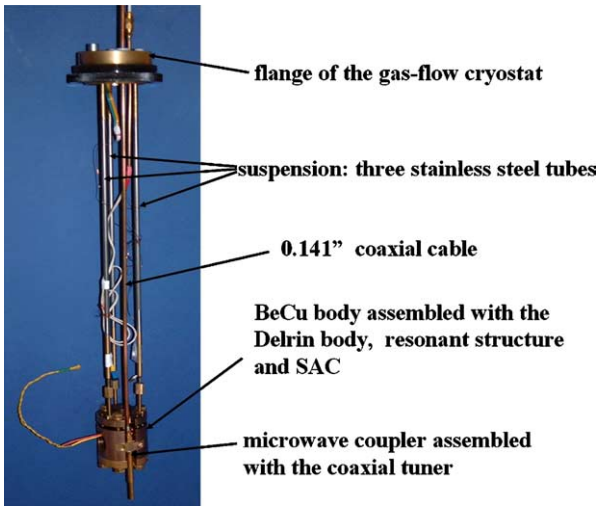

Fig. 7. The assembled DR-based high-pressure ESR probe attached to the flange of the continuous gas-flow cryostat, Model CF1200 (Oxford Instruments).

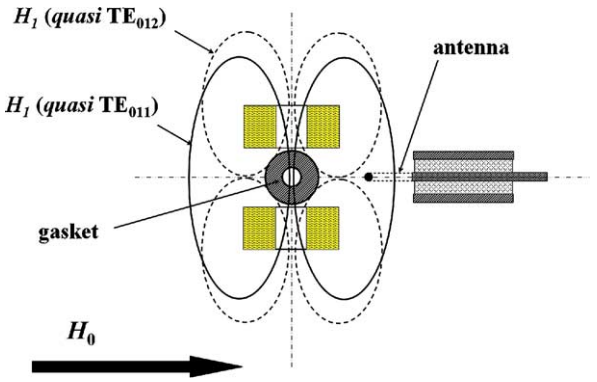

Fig. 8. Simplified cross-sectional view of the modal distribution patterns for the two lowest modes of cylindrical symmetry observed for the *wide-stretched* double-stacked DR. Solid lines tentatively show the distribution of the H_1 component for the lowest axial *quasi* TE_{011} mode. Broken lines depict the distribution of the H_1 component for the higher axial *quasi* TE_{012} mode.

posts (M4) firmly anchored to the BeCu upper lid (Fig. 5A) serve to connect the BeCu body to three stainless-steel tubes (4 mm DIA), which form the suspension of the high-pressure ESR probe (Fig. 7). The upper terminations of these stainless-steel tubes are anchored in the bottom face of the cryostat flange. The system was successfully checked at cryogenic temperatures, thus surviving numerous temperature cycles from room temperature to ~10 K [44]. After several experiments, however, some traces of material fatigue occurred in the Derin body (small cracks of plastic around the microwave cutoff elements).

2.4. Topology of the microwave resonant modes of the double-stacked DR

The *wide-stretched* double-stacked DR structure employed in this design resonates in two easily distinguishable microwave modes of cylindrical symmetry. As mentioned before, the lower-frequency mode, herein referred to as the ESR-active mode *quasi* TE_{011}, resonates around 9.20 GHz. The higher-frequency mode, which we refer to as *quasi* TE_{012}, resonates at ~9.4 GHz. The modal distribution patterns for these two modes are schematically shown in Fig. 8.

As can be seen in Fig. 8, the higher axial *quasi* TE_{012} mode has a nodal point for the tangential H_1 component in the center of the resonant structure (i.e., at the sample location in the gasket hole). In contrast, the lowest *quasi* TE_{011} mode has a non-vanishing H_1 component at the sample location, which is depicted by ovals marked by solid lines in Fig. 8. A tangential portion of the axial component of H_1 slightly bends upon the sample hole in the gasket, which gives rise to the ESR activity of the *quasi* TE_{011} mode. A more detailed discussion of the topology of the ESR-active *quasi* TE_{011} mode for the double-stacked DR can be found in [42,43]. The theoretical model elaborated for the double-stacked DR in reference 42 yields the following resonant frequencies, f_0, for the ESR-active mode (*quasi* TE_{011}): 9.16 and 9.27 GHz, for the Rexolite-filled and empty microwave shield, respectively. For the higher mode *quasi* TE_{012}, herein referred to as ESR-silent, the theoretical model yields $f_0 = 9.35$ GHz (while assuming empty microwave shield). The theoretical estimation, however, does not take into account perturbations due to the presence of additional elements belonging to the SAC, such as the metallic fragments of the pistons, sapphire anvils, and pressure gasket. The presence of the above-mentioned elements shifts the resonant frequency to slightly higher values of 9.2 and 9.45 GHz, for the *quasi* TE_{011} and *quasi* TE_{012} modes, respectively.

The measured loaded Q_L-factor values for the ESR-active and ESR-silent modes were different. In particular, for the *quasi* TE_{012} mode we observed higher Q_L-factor values (~2500) than for the ESR-active *quasi* TE_{011} mode ($Q_L \sim 1200$). As can be deduced from Fig. 8, for the *quasi* TE_{012} mode the overall topology of the modal distribution pattern is only slightly perturbed by the presence of the mechanical elements of the SAC. In contrast, for the *quasi* TE_{011} mode (ESR-active), the effective perturbation of the modal distribution pattern is considerably larger, which results in lower Q_L-factor values.

3. Ruby calibration of the hydrostatic pressure

The measurement of sample pressure in the cylindrical hole of the gasket is performed using the ruby-fluorescence technique. The intense fluorescence of the ruby's *R*-lines (Cr^{3+}-related luminescence in Al_2O_3 with Cr^{3+} impurities) is sensitive to the change of interatomic distances resulting from the application of the external pressure. In the experimental setup presented in this work, the pressure-induced shift of *R*-lines was monitored using a commercially available high-pressure measurement system Dilor, Model SP300 (Dilor SA, Lille, France). This sys-

tem consists of an argon laser and a multichannel spectrophotometer equipped with a photodiode array detector. The laser beam (30 μm in diameter) from the Dilor's argon laser is routed to a small ruby crystal placed next to the sample in the hydrostatic fluid that fills the gasket hole. The green laser light, $\lambda = 514.5$ nm, excites transitions within the ruby Cr^{3+} electronic manifold, which gives rise to the red fluorescence around $\lambda = 694$ nm. As can be seen in Fig. 1, the BeCu lower piston and BeCu lower lid have conical openings of a large aperture, which makes it possible to photo-excite the ruby crystal in the sample compression chamber as well as it facilitates routing of the red ruby luminescence back to the Dilor's multichannel photodiode array detector. A commercial CCD-camera in combination with a video monitor Panasonic, Model WV-5340, was used for visualization of the gasket hole. We found this setup particularly useful to track down the tiny ruby crystal in the sample hole, as well as for a general inspection of the gasket after the assembly of the system and during the subsequent incremental changes of pressure. Illumination of the gasket was achieved by shining the white light from a standard halogen source directly on the lateral surface of sapphire pistons. To this end, the microwave coupler was detached from the BeCu body and the termination of a flexible light fiber was then inserted into the cylindrical antenna entrance port.

4. Performance of the high-pressure ESR probe

4.1. ESR characteristics of the double-stacked DR resonant structure

The overall performance of the high-pressure ESR system was checked using a standard sample, 2,2-diphenyl-1-picrylhydrazyl radical (DPPH), from Sigma.

The polycrystalline DPPH yields a strong, exchange-narrowed ESR line with $g = 2.0036$ and $\Delta H_{pp} = 1.65$ G at room temperature and pressure. A small amount of powdered DPPH (less than 0.1 mg) was wrapped up in a tiny flake of PTFE tape (thickness 50 μm, surface less than 4 mm^2), thus forming a small sphere with the diameter of less than ~0.3 mm. Subsequently, it was positioned adjacent to a small ruby crystal in the sample compression chamber (0.9 mm in diameter). Then, the gasket hole was filled with distilled water and the whole system was assembled for performing ESR measurements. The hydrostatic pressure was set to ~0.1 GPa. Since the solubility of DPPH in water is negligible, for performing test measurements with the standard sample, we found the aqueous milieu more adequate than that of oils or organic solvents.

To compare the ESR sensitivity, the gasket containing the DPPH sample was removed from the DR-based high-pressure ESR probe and inserted into the regular TE_{102}. As can be seen in Fig. 9, the overall sensitivity of the DR-based system is only ~3 times less than that yielded by a commercial TE_{102} cavity operating at room pressure.

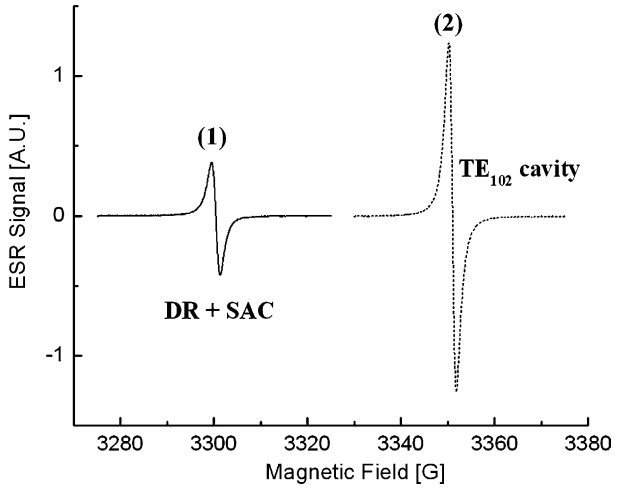

Fig. 9. Sensitivity test of DR-based high-pressure ESR probe. Spectrum **1** (solid line) was acquired for a small speck of DPPH positioned in the gasket hole of the SAC in the fully assembled high-pressure probe. The sample compression chamber of the gasket was filled with distilled water and the hydrostatic pressure was set to ~0.1 GPa. Spectrum **2** (dashed line) was acquired in the TE_{102} cavity for the same DPPH sample. The gasket containing the DPPH sample was removed from the SAC and positioned in the cavity. The same instrumental settings were used for both experiments: microwave power 2 mW, 100 kHz modulation 0.25 G, time constant 0.1 ms, sweep width 20 G. The microwave frequencies were 9.25 and 9.40 GHz for the DR-based high-pressure ESR probe and the TE_{102} cavity, respectively. The gasket ID was 0.6 mm.

The shift of the resonant fields for the ESR traces shown in Fig. 9 was due to the different microwave resonant frequencies, which were 9.25 and 9.40 GHz, for the DR-based high-pressure ESR probe and the TE_{102} cavity, respectively. It is also worth noticing that the Q_L-factor of the TE_{102} cavity was of ~3000, whereas the Q_L-factor measured for the double-stacked DR-based resonant structure in the fully assembled high-pressure ESR probe was of ~1200.

The position of the microwave antenna in the resonant structure (see Fig. 8) favors the *quasi* TE_{011} mode (ESR-active). However, for exactly the same antenna position, the *quasi* TE_{012} mode is also excited. As shown in Fig. 8, this mode has a nodal point for the H_1 component in the center of the resonant structure. Interestingly, however, for the test DPPH sample positioned in the center of the resonant structure (i.e., in the gasket of the SAC) and for the same instrumental settings, this mode also yielded an ESR signal, which was ca. 10 times lower than that observed for the *quasi* TE_{011} mode (ESR-active).

The corresponding ESR traces for the test DPPH sample acquired for both modes are shown in Fig. 10. The two weak features on the left- and right-hand sides of the DPPH line belong to the characteristic ESR spectrum of Mn^{2+} centers in MgO/MnO from a reference sample, which was also present in the resonant structure. Due to the narrow field scan of 150 G, only two central features of the Mn^{2+} hyperfine sextet can be seen in the ESR traces presented in Fig. 10. A short section of 0.6-mm ID and 0.87-mm OD quartz capillary, containing a small amount of polycrystalline MgO/MnO, was inserted along the cylin-

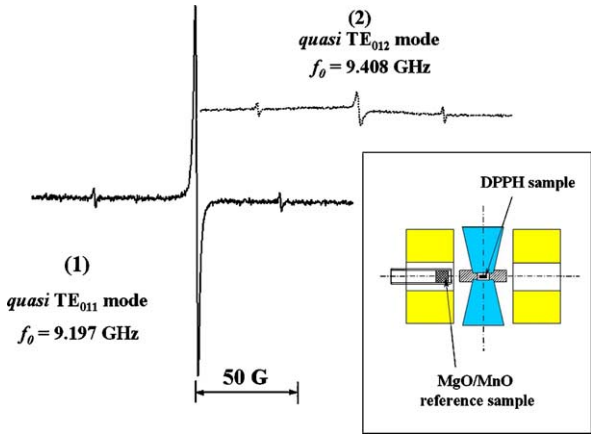

Fig. 10. Sensitivity comparison for the two resonant modes, *quasi* TE_{011} and *quasi* TE_{012}, which are supported by the double-stacked DR-based resonant structure. Two ESR traces are shown: spectrum **1** (solid line) and spectrum **2** (dotted line) for the *quasi* TE_{011} and *quasi* TE_{012} modes, respectively. The instrumental settings were: microwave power 2 mW, 100 kHz modulation 0.25 G, time constant 0.1 ms, sweep width 150 G. The microwave frequencies were 9.197 and 9.408 GHz for the ESR-active and ESR-silent modes, respectively. Inset: schematically shown are the locations of the small speck of DPPH and MgO/MnO reference sample.

drical axis of the resonant structure and positioned close to the gasket (as shown in inset to Fig. 10). We found it useful to monitor the ESR signal from this reference sample while performing regular high-pressure experiments.

Therefore, in combination with the reference MgO/MnO sample, it can be used for checking the status of the resonant structure, especially when the *quasi* TE_{011} mode (ESR-active) is strongly distorted by the pressure-deformed gasket.

4.2. High-pressure ESR study of spin-relaxation mechanism in K_1C_{60}

The newly developed high-pressure ESR apparatus was used for high-pressure studies of the spin-relaxation mechanism in an orthorhombic phase conducting polymer, K_1C_{60}. This compound is a representative of fullerene-based alkali-doped materials, A_1C_{60}, where A = K, Rb, Cs. Similar to the other compounds belonging to the A_1C_{60} family, while slowly cooled down below 400 K, K_1C_{60} undergoes a phase transition from a cubic *fcc* phase to a conducting orthorhombic phase [46]. The earlier studies of the magnetic susceptibility and electrical transport properties confirmed the metallic-type behavior of the orthorhombic phase K_1C_{60} in a wide range of temperatures (50–350 K) [47].

K_1C_{60} sample was prepared according to the procedure described in [47]. Small amount of powdered K_1C_{60} was wrapped up in a tiny flake of PTFE and positioned into the gasket hole using the same procedure as described above for the DPPH test sample. Paraffin oil was used as the pressure-transmission medium in this experiment.

At room temperature and pressure the fine powder of the conducting K_1C_{60} sample yields a strong and relatively narrow (ΔH_{pp} ~4.5 G) signal, which is customarily ascribed to conduction electron spin resonance (CESR) [16]. The CESR line shape of the fine-powdered K_1C_{60} is very close to Lorentzian. The high-spin susceptibility of the conducting orthorhombic phase of K_1C_{60} is due to the *quasi*-1D electronic structure of the polymerized C_{60} chains [47,48]. This also results in an unconventional spin relaxation and pressure dependence of the CESR linewidth [16].

The evolution of the CESR linewidth as a function of hydrostatic pressure for K_1C_{60} is shown in Fig. 11A.

The pressure-induced CESR line broadening shown in Fig. 11A can be understood in terms of an enhanced electron spin-flop probability between the polymeric chains in the orthorhombic-phase K_1C_{60}. For 1D-conducting materials the CESR linewidth (ΔH_{pp}) can be expressed as $\Delta H_{pp} \sim (\Delta g)^2/\tau_\perp$, where Δg represents the difference between the measured *g*-factor and that of the free electron, g_e, whereas $\tau_\perp$ denotes the inter-chain spin-scattering time. Since Δg is practically independent of pressure for 1D materials, $\tau_\perp$ should diminish to accommodate for the observed pressure-induced broadening of the CESR line. The linear increase of ΔH_{pp} with increasing hydrostatic pressure shown in Fig. 11B points to the spin-relaxation mechanism that is governed by the inter-chain spin-flop mechanism be-

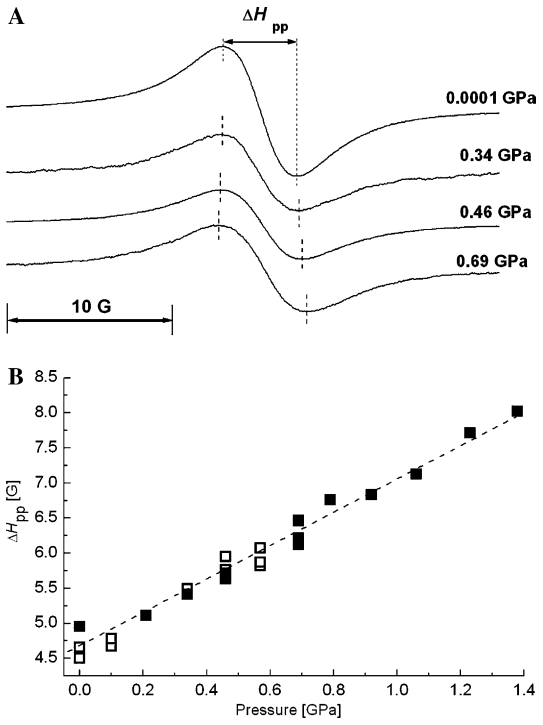

Fig. 11. Evolution of the peak-to-peak CESR linewidth (ΔH_{pp}) for the polycrystalline sample of K_1C_{60} at room temperature (300 K) as a function of pressure. (A) Example CESR spectra of K_1C_{60} acquired at different hydrostatic pressures. (B) The dependence of the peak-to-peak CESR linewidth (ΔH_{pp}) as a function of hydrostatic pressure. Open squares correspond to the experimental points taken in the helium-gas operating ESR high-pressure system [16]. Black squares are experimental points obtained using the DR-based high-pressure ESR probe. Paraffin oil was used as the pressure-transmitting medium in the gasket of the SAC.

tween the conducting chains, thus confirming the hypothesis of the existence of the polymeric chains and *quasi*-1D-conducting character of K_1C_{60} [48].

4.3. The paramagnetic baseline of the DR-based high-pressure ESR system

Knowing the overall paramagnetic background of the probe is of great importance while performing experiments on various paramagnetic systems. Therefore, in addition to acquiring the ESR spectra in narrow field scans (around $g \sim 2$), we also recorded spectra using wide sweeps of the magnetic field.

The exemplary ESR spectrum of the paramagnetic background of the double-stacked DR is shown in Fig. 12A. In this trace, in addition to a strong narrow signal from the sample located in the gasket hole (CESR signal of K_1C_{60}), one can also distinguish a broad paramagnetic background related to the ESR signal of the high-dielectric ceramics. The spectral features and intensity of the paramagnetic background depend on the ceramic's purity [43,45].

In the signal baseline one can also distinguish a relatively narrow ESR feature ($\Delta H_{pp} \sim 20$ G) occurring at the resonant field, $H_{res} = 1892$ G. This latter signal is associated with the presence of trivalent chromium (Cr^{3+}) ions in the sapphire anvils.

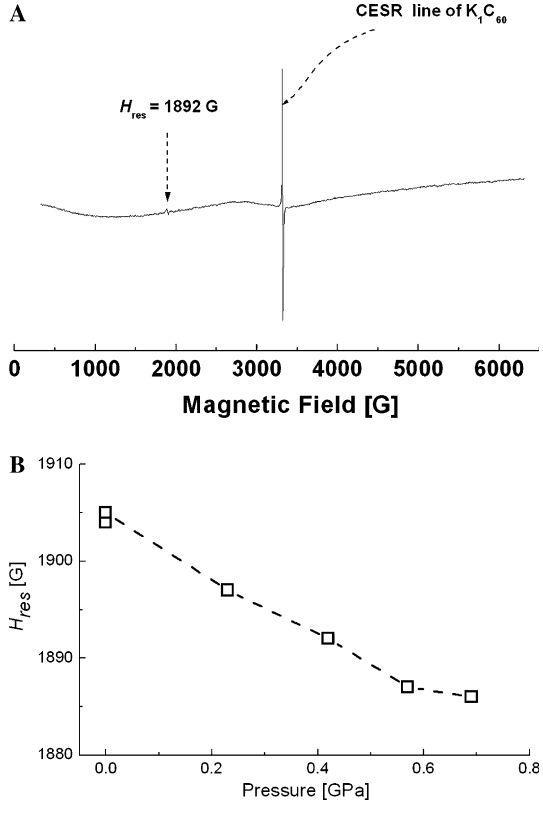

Fig. 12. The paramagnetic background of the DR-based high-pressure ESR probe. (A) The 6000 G-wide sweep background trace of the high-pressure ESR probe. The powdered K_1C_{60} is located in the gasket hole and pressurized to 0.42 GPa. The small peak at 1892 G reveals the presence of Cr^{3+} centers in the sapphire anvils. (B) The dependence of the resonant field, H_{res}, for the trivalent chromium (Cr^{3+}) impurity in sapphire anvils as a function of hydrostatic pressure.

The Cr^{3+} ion is an $S = 3/2$ spin system due to three unpaired electrons on the partially filled 3d shell. Since the *c*-axis of the sapphire pistons is oriented perpendicular to the external magnetic filed B_0, the allowed $\Delta M_s = \pm 1$ electron–spin transitions within the $M_s = \pm 1/2 \Longleftrightarrow \pm 3/2$ manifold yield the characteristic ESR feature around $H_{res} = 1890$ G [49]. Sakai and Pifer [35] also reported the presence of a similar Cr^{3+}-related feature in the ESR baseline, since their system employed the sapphire posts to transfer the mechanical stress to the diamond anvils.

We noticed that the Cr^{3+}-related feature, which is far away from the most frequently used spectral region around $g \sim 2$, can also be used as a crude indicator of the mechanical strain in the sapphire anvils.

The dependence of the resonant field, H_{res}, for the transition $M_s = \pm 1/2 \Longleftrightarrow \pm 3/2$ as a function of the hydrostatic pressure in the gasket is shown in Fig. 12B. It is worthwhile to mention that Cr^{3+}-related feature also broadens with the increasing mechanical strain in the anvils. At pressures higher than 0.8 GPa, this line was smeared out due to the strongly non-homogeneous strain distribution in the sapphire anvils.

5. Summary and outlook

We reported the technical aspects and an exemplary application of the novel technology that combines the sensitive DR-based resonant structure with a well-established technique of the high-pressure gasketed anvil cells. The gasketed sapphire anvil cell (SAC) was used as a pressure-generating component in this design and the hydrostatic pressure in the gasket hole was ruby-calibrated. Due to a considerable difference in prices of sapphire anvils (~$10.00 a pair) and diamond anvils (~$5000.00 a pair) and since both types of anvils brake sometimes while performing the experiments, the combination of the double-stacked DR with the SAC offers a cheaper alternative in maintenance costs to the systems that employ diamond-anvil cells. Yet, the DR-based high-pressure ESR system equipped with the SAC provides a useful range of pressures up to ~2 GPa for performing ESR experiments under high-hydrostatic pressure. There is, however, a considerable potential in extending the present pressure range by incorporating sapphire anvils with beveled edges and by improving the pistons' guidance and alignment. In particular, the latter goal can be achieved by elongating the cylindrical holes that provide guidance for the pistons of the SAC.

Since the two essential elements of the microwave probe, i.e., the Rexolite resonator body and Delrin body, were made from plastic materials, the whole resonant could easily be machined and was also transparent to the regular 100 kHz magnetic filed modulation. However, since we observed traces of thermal–mechanical fatigue of the Delrin-made piece after several exposures to cryogenic tempera-

tures, we envisage re-designing of this element by using other, low-temperature dedicated materials, like, for example, robust fluorocarbon-based polymer, Kel-F^{R}, or machinable glass ceramics, Macor^{R}.

Small external dimensions of the assembled system enabled one to insert the high-pressure ESR probe into a commercial continuous gas-flow cryostat. Since the frequency temperature coefficient (τ_f) of the high-dielectric ceramic material used in our design was close to zero (characteristic code 'C' in the MuRata Resomics manufacturer's data sheet of Model DRT065R020C029A dielectric resonators), we could employ the probe in a wide range of temperatures (10–300 K), while encountering only minor changes in the resonant frequency and tuning [44].

The overall dimensions of the microwave heart and essential mechanical parts (including the BeCu body) are small. Therefore, it is possible to transfer the high-pressure ESR probe into a regular laboratory glove-box, thus enabling one to load samples under anaerobic conditions.

The newly developed high-pressure ESR probe was successfully tested with both the ESR standard sample (DPPH) and while elucidating mechanisms of spin relaxation in low-dimensional systems of K_1C_{60}.

For small polycrystalline samples, the DR-based high-pressure system offers the signal-to-noise ratio that is only $\sim$3 times less than that yielded by commercially available ESR cavities operating at room pressure.

Due to the possibility of using water as the pressure-transmitting medium, the design presented here might be of importance for performing high-pressure ESR studies of aqueous samples or samples suspended in aqueous milieus.

Acknowledgments

The authors particularly like to acknowledge Mr. Michel Longchamp from the Machine Shop of the EPFL for his frequent technical assistance. This work has also been partly supported by the by the Polish KBN Grant #2-PO3B-090-19 (A.S.) and the grant No. G1MA-CI-2002-4017 (CEPHEUS) of the European Commission (A.S.).

References

[1] G.B. Benedek, Magnetic Resonance at High Pressure, Interscience, NY, 1963.
[2] J.A.S. Smith, High Pressure Physics and Chemistry, vol. 2, Academic Press, NY, 1963, p. 293.
[3] C.P. Poole Jr., Electron Spin Resonance: A Comprehensive Treatise on Experimental Techniques, Interscience Publishers, NY, 1967, p. 257.
[4] T.I. Alaeva, L.F. Vereshchagin, J.A. Timofeev, E.N. Yakovlev, Cell for investigation of spectra of electron resonance by quasi-hydrostatic pressure up to 100 kilobar, Prib. Tekh. Eksp. 1 (1971) 206.
[5] J. Stankowski, A. Gałęzewski, M. Krupski, S. Waplak, H. Gierszal, Microwave resonators for EPR studies at high hydrostatic pressure, Rev. Sci. Instrum. 47 (1976) 128.
[6] I.P. Kaminow, R.V. Jones, Pressure dependence of microwave resonance properties of some spinel and garnet ferrites, Phys. Rev. 123 (1961) 1122.
[7] A.B. Wolbarst, High pressure, low temperature ENDOR-EPR cavity, Rev. Sci. Instrum. 47 (1976) 255–257.
[8] M.W. Walsh, N. Blombergen, Paramagnetic resonance of nickel fluosilicate under high hydrostatic pressure, Phys. Rev. 107 (1957) 904–905.
[9] M. Krupski, Corundum-filled resonator systems for high-pressure and low-temperature electron paramagnetic resonance studies, Rev. Sci. Instrum. 67 (1996) 2894–2898.
[10] M. Jaworski, K. Chęciński, W. Bujnowski, S. Porowski, High-pressure EPR cavity, Rev. Sci. Instrum. 49 (1978) 383–384.
[11] Sienkiewicz, M. Jaworski, High hydrostatic pressure ESR manostats, High Pressure Res. 5 (1990) 877–879.
[12] J. Szczepek, A. Sienkiewicz, High-pressure system for EPR measurements, in: W. Trzeciakowski, (Ed.), Proceedings of the Joint XV AIRAPT and XXXIII EHPRG International Conference on High Pressure Science and Technology, Warsaw, Sept. 11–15, 1995. 1966, pp. 57–59.
[13] J.-P. Michaut, J. Roncin, A. Sienkiewicz, Temperature and pressure-dependence studies of the motions of the $^{+}NH_3$ radical trapped in gamma-irradiated ammonium-perchlorate single crystal, Mol. Cryst. Liq. Cryst. 53 (1979) 281–289.
[14] H. Reichelt, W. Windsch, A. Sienkiewicz, Pressure and temperature-dependence of the local order parameter in Mn^{2+}-doped tris-sarcosine calcium-chloride, Ferroelectrics 34 (1981) 195–201.
[15] O. Chauvet, A. Sienkiewicz, L. Forró, L. Zuppiroli, High-pressure electron–spin dynamics in disordered conducting polymers, Phys. Rev. B 52 (1995) R13118–R13121.
[16] L. Forró, G. Baumgartner, A. Sienkiewicz, S. Pekker, O. Chauvet, F. Beuneu, H. Alloul, Pressure and disorder effect on the magnetic properties of the A_1C_{60} conductors, fullerenes and fullerene nanostructures, in: H. Kuzmany, J. Fink, M. Mehring, S. Roth (Eds.), Proceedings of the International Winter School on Electronic Properties of Novel Materials, Kirchberg, Tyrol, Austria, 2–9 March, 1996, World Scientific, 1996, pp. 102–109.
[17] N. Čegar, F. Simon, G. Baumgartner, A. Sienkiewicz, L. Forró, B. Ruzicka, L. Degiorgi, L. Mihály, Electronic properties of the Na_2AC_{60} family (A = K, Rb, Cs), in: H. Kuzmany, J. Fink, M. Mehring, S. Roth (Eds.), Proceedings of the International Winterschool on Electronic Properties of Novel Materials—Science and Technology of Molecular Nanostructures, Kirchberg, March 1999, American Institute of Physics, Woodbury, New York, 1999, pp. 64–68.
[18] F. Bridges, S. Ready, M. Morgan, High-pressure multimode resonator system for high microwave-frequencies up to 215 GHz, Rev. Sci. Instrum. 55 (1984) 75–78.
[19] H.M. Nelson, D.B. Larson, J.H. Gardner, Very high pressure effects upon ESR spectrum of ruby, J. Chem. Phys. 47 (1967) 1994.
[20] J.D. Barnett, S.D. Tyagi, H.M. Nelson, System for ESR measurements at hydrostatic pressures to 60 kilobars, Rev.Sci. Instrum. 49 (1978) 348–355.
[21] G.J. Piermarini, S. Block, Ultrahigh pressure diamond-anvil cell and several semiconductor phase-transition pressures in relation to fixed-point pressure scale, Rev. Sci. Instrum. 46 (1975) 973–979.
[22] A. Jayaraman, Diamond anvil cell and high-pressure physical investigations, Rev. Mod. Phys. 55 (1983) 65.
[23] A. Jayaraman, Ultrahigh pressures, Rev. Sci. Instrum. 57 (1986) 1013–1031.
[24] D.J. Dunstan, I.L. Spain, The technology of diamond anvil high pressure cells. 1. Principles design and construction, J. Phys. E—Sci. Instrum. 22 (1989) 913–923.
[25] B.A. Weinstein, G.J. Piermarini, Raman-scattering and phonon dispersion in Si and GaP at very high pressure, Phys. Rev. B 12 (1975) 1172–1186.
[26] D. Schiferl, S.K. Sharma, T.F. Cooney, S.Y. Wang, K. Mohanan, Multichannel Raman-spectroscopy system for weakly scattering materials at simultaneous high-pressures and high-temperatures, Rev. Sci. Instrum. 64 (1993) 2821–2827.

[27] C.H. Whitfield, E.M. Brody, W.A. Bassett, Elastic-moduli of NaCl by Brillouin-scattering at high pressure in a diamond anvil cell, Rev. Sci. Instrum. 47 (1976) 942–947.
[28] M.A. Baublitz, V. Arnold, A.L. Ruoff, Energy dispersive-X-ray diffraction from high pressure polycrystalline specimens using synchrotron radiation, Rev. Sci. Instrum. 52 (1981) 1616–1624.
[29] H.K. Mao, R.J. Hemley, Y. Wu, A.P. Jephcoat, L.W. Finger, C.S. Zha, W.A. Basset, High-pressure phase diagram and equation of state of solid helium from single-crystal X-ray diffraction to 23.3 GPa, Phys. Rev. Lett. 60 (1988) 2649–2652.
[30] G.R. Hearne, M.P. Pasternak, R.D. Taylor, Fe-57 Mössbauer spectroscopy in a diamond-anvil cell at variable high-pressures and cryogenic temperatures, Rev. Sci. Instrum. 65 (1994) 3787–3792.
[31] D. Erskine, P.Y. Yu, G. Martinez, Technique for high-pressure electrical-conductivity measurement in diamond anvil cells at cryogenic temperatures, Rev. Sci. Instrum. 58 (1987) 406–411.
[32] M.F. Li, P.Y. Yu, E.R. Weber, W. Hansen, Photocapacitance study of pressure-induced deep donors in GaAs-Si, Phys. Rev. B 36 (1987) 4531–4534.
[33] A.L. Ruoff, H. Xia, Q. Xia, The effect of a tapered aperture on x-ray diffraction from a sample with a pressure gradient: studies on three samples with a maximum pressure of 560 GPa, Rev. Sci. Instrum. 63 (1992) 4342–4348.
[34] M.I. Eremets, V.V. Struzhkin, A.N. Utjuzh, Miniature high-pressure cells for high magnetic-field applications, Physica B 211 (1995) 369–371.
[35] N. Sakai, J.H. Pifer, Electron paramagnetic resonance at high-pressure using a diamond anvil cell, Rev. Sci. Instrum. 56 (1985) 726–732.
[36] S.E. Bromberg, I.Y. Chan, Enhanced sensitivity for high-pressure EPR using dielectric resonators, Rev. Sci. Instrum. 63 (1992) 3670–3673.
[37] J.K. Plourde, C.L. Ren, Application of dielectric resonators in microwave components, IEEE Trans. Microwave Theory Tech. 29 (1981) 754–770.
[38] H. Hughes, D.M. Iddles, I.M. Reaney, Niobate-based microwave dielectrics suitable for third generation mobile phone base stations, Appl. Phys. Lett. 79 (2001) 2952–2954.
[39] R.W. Dykstra, G.D. Markham, A dielectric sample resonator design for enhanced sensitivity of EPR spectroscopy, J. Magn. Reson. 69 (1986) 350–355.
[40] W.M. Walsh, L.W. Rupp, Enhanced electron spin resonance sensitivity using a dielectric resonator, Rev. Sci. Instrum. 57 (1986) 2278–2279.
[41] A. Sienkiewicz, K. Qu, C.P. Scholes, Dielectric resonator-based stopped-flow electron paramagnetic resonance, Rev. Sci. Instrum. 65 (1994) 68–74.
[42] M. Jaworski, A. Sienkiewicz, C.P. Scholes, Double-stacked dielectric resonator for sensitive EPR measurements, J. Magn. Reson. 124 (1997) 87–96.
[43] A. Sienkiewicz, M. Jaworski, B.G. Smith, P.G. Fajer, C.P. Scholes, Dielectric resonator-based side-access probe for muscle fiber EPR study, J. Magn. Reson. 143 (2000) 144–152.
[44] S. Garaj, T. Kambe, L. Forró, A. Sienkiewicz, M. Fujiwara, K. Oshima, Polymer phase of the tetrakis (dimethylamino)ethylene-C_{60} organic ferromagnet, Phys. Rev. B 68 (2003) 144430–144437.
[45] G. Lassmann, P.P. Schmidt, W. Lubitz, An advanced EPR stopped-flow apparatus based on a dielectric ring resonator, J. Magn. Reson. 172 (2005) 312–323.
[46] J. Winter, H. Kuzmany, Potassium-doped fullerene K_XC_{60} with $X = 0,1,2,3,4$, and 6, Solid Sate Commun. 84 (1992) 935–938.
[47] F. Bommeli, L. Degiorgi, P. Wachter, O. Legeza, A. Jánossy, G. Oszlanyi, O. Chauvet, L. Forró, Metallic conductivity and metal-insulator transition in $(AC_{60})_n$ (A = K, Rb, and Cs) linear polymer fullerides, Phys. Rev. B 51 (1995) 14794–14797.
[48] S. Pekker, L. Forró, L. Mihály, A. Jánossy, An orthorhombic A_1C_{60}—a conducting linear alkali fulleride polymer? Solid State Commun. 90 (1994) 349–352.
[49] J. Weber, Masers, Rev. Mod. Phys. 31 (1959) 671–681.